

Optimization potentials for the absorber and the generator of an ammonia-water absorption heat pump

Nico MIRL, Klaus SPINDLER

Institute for Building Energetics, Thermotechnology and Energy Storage (IGTE), University of Stuttgart, Pfaffenwaldring 6, Stuttgart, 70569, Germany, Nico.Mirl@igte.uni-stuttgart.de

ABSTRACT

Experimental investigations to identify optimization potentials of an ammonia-water absorption heat pump are performed. In this heat pump, both the absorber and the generator are designed as plate heat exchangers. At the inlet of the absorber, the weak solution is sprayed through a nozzle into the refrigerant vapor, thus creating a high surface for the mass transfer. The advantages of this system are a compact design and a low refrigerant filling quantity.

The aim of these investigations is to identify and classify optimization potentials in heat and mass transfer in the absorber and generator. The potentials in heat transfer are determined using calculated temperature profiles. For an analysis of the mass transfer, the ammonia mass fractions of the strong and the weak solution are calculated with measured densities. By comparison with the theoretically possible ammonia mass fractions, a classification in the areas of heat or mass transfer is carried out for further optimization.

Keywords: Absorber, Absorption System, Ammonia-Water, Generator, Heat Transfer, Mass Transfer, Optimization, Plate Exchanger

1. INTRODUCTION

In German district heating systems, operating temperatures up to 140 °C are available (Paar et al. 2013) while in customer heating systems, temperatures up to 70 °C are required. An improved cooling of the district heating water leads to a reduction of the return temperature. One promising opportunity to achieve an improved cooling is to use the high temperature of the district heating flow to power an absorption heat pump with the working pair ammonia-water and to use the return as heat source for the evaporator (Mirl et al. 2018b). Due to safety regulations for the place of installation, the filling quantity of the absorption heat pump should be less than 10 kg ammonia.

The size and filling quantity of the absorption heat pump is highly affected by the generator. In ammonia-water absorption systems, a vessel-type generator is typically in use (Said et al. 2016; Staedter and Garimella 2018; Aprile et al. 2016). By using a plate heat exchanger as generator, Müller and Spindler (2013) reduced the ammonia filling quantity from 15 kg to 4 kg. However, the coefficient of performance of the absorption system decreased from 0.65 to 0.6. In order to improve the efficiency of the absorption system, the potentials in heat and mass transfer of the plate-type generator have to be investigated.

The absorber mainly influences the efficiency of the whole absorption process (Mittermaier and Ziegler 2015). Many different types of absorbers are studied in literature, such as falling film absorbers (Castro et al. 2009; Triché et al. 2017), bubble absorbers (Cerezo et al. 2010) and spray absorbers (Said et al. 2016; Müller and Spindler 2013; Venegas et al. 2005). The latter absorber type seems to be very compact, due to a high surface for mass transfer within the spray. Müller and Spindler (2013) built a spray absorber where the weak solution is direct sprayed into a plate heat exchanger; the high surface for mass transfer of the spray is combined with the high surface for heat transfer of a plate heat exchanger, working as a falling film absorber.

In the present work, an ammonia-water absorption heat pump with 30 kW heating power has been investigated experimentally. The focus has been on the analysis of the current state of the generator and the spray absorber of the ammonia-water absorption heat pump as well as on the identification and classification of the main optimization potentials. For both, absorber and generator, commercial plate heat exchangers are used, due to their compactness and low costs (Müller and Spindler 2013).

2. EXPERIMENTAL SETUP

The schematic design of the absorption heat pump is shown in Figure 1. The refrigerant vapor (1) is liquefied in the condenser where a part of the useful heat \dot{Q}_{cond} is extracted from the process. The refrigerant storage tank (2) is used for the intermediate storage of liquid refrigerant. This increases the operating range of the absorption heat pump and compensates temperature fluctuations of the external circuits. The refrigerant heat exchanger increases the efficiency of the process: the liquid refrigerant is subcooled after the condenser (3→4) and the refrigerant vapor (6→7) is superheated. Via the refrigerant expansion valve, the pressure of the liquid refrigerant is reduced to the low pressure of the heat pump (4→5). At the low pressure, the refrigerant can be evaporated at a low temperature level (5→6). At the inlet of the absorber, the refrigerant vapor (7) is mixed with the weak solution (8) in the absorber, resulting in the absorption of the refrigerant. In this process, the absorption heat \dot{Q}_{abs} is released; therefore, this heat must be transferred to the heating system at a medium temperature level. At the end of the absorption process, the strong solution has an increased ammonia mass fraction ξ_{ss} and is in liquid state (9). The liquid strong solution (9) is led into a pump storage tank. The level of the strong solution in this tank (10) is controlled at a constant value. Via a solution pump, the strong solution is adjusted to the high pressure (11). In order to increase efficiency, a solution heat exchanger is used for internal heat recovery between strong solution (11→12) and weak solution (19→20). Then, the preheated strong solution flows through the dephlegmator (13→14), where internal heat recovery from the refrigerant vapor to the strong solution takes place. Due to the preheating of the strong solution, a two-phase mixture of liquid strong solution and refrigerant gas enters the generator storage tank (14). A connecting pipe (16) between the storage tank and the dephlegmator transports refrigerant vapor to the dephlegmator (17). The liquid strong solution flows to the generator where heat \dot{Q}_{gen} at a high temperature level is used to evaporate the strong solution (15) partially. In the generator separator, the two-phase flow is separated into refrigerant vapor (18) and weak solution (19). The latter is fed back to the absorber (19→20→8) and reused for the absorption process.

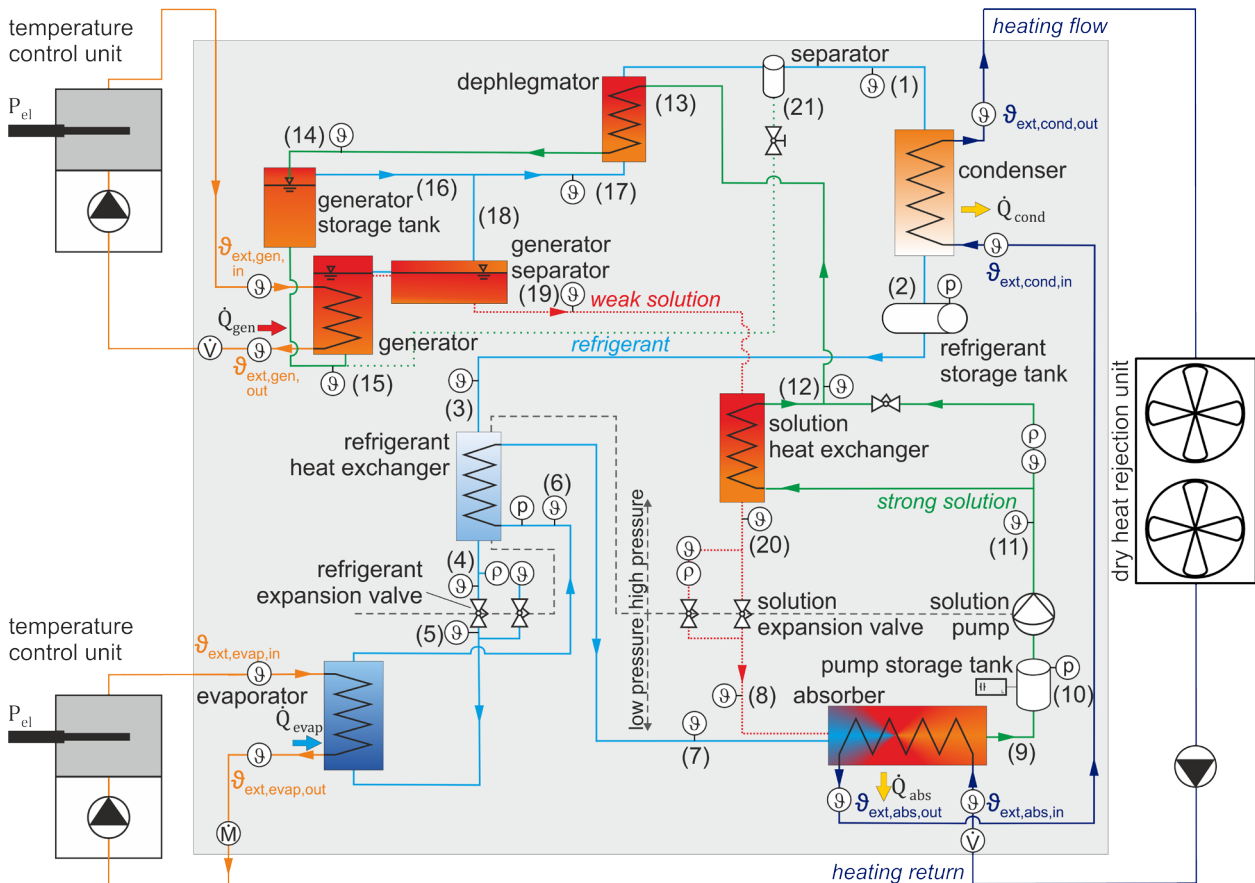


Figure 1: schematic design of the ammonia-water absorption heat pump with measuring locations

Table 1. Uncertainty and quantity of the used measurement

Sensors type	Quantity	Uncertainty
internal fluid temperature (Pt100 1/3B)	14	$\pm 1/3 \cdot (0.3 \text{ }^\circ\text{C} + (0.005) \text{ }^\circ\text{C}^{-1} \cdot \vartheta)$
external fluid temperature (Pt100 1/10B)	8	$\pm 1/10 \cdot (0.3 \text{ }^\circ\text{C} + (0.005) \text{ }^\circ\text{C}^{-1} \cdot \vartheta)$
low pressure (0...10 bar)	2	$\pm 0.008 \text{ bar}$
high pressure (0...25 bar)	1	$\pm 0.25 \text{ bar}$
density internal Coriolis flow meter	3	$\pm 0.5 \text{ kg m}^{-3}$
fluid temperature internal Coriolis flow meter	3	$\pm 0.5 \text{ }^\circ\text{C} + 0.005 \text{ }^\circ\text{C}^{-1} \cdot \vartheta$

The refrigerant vapor extracted from the generator is no pure ammonia due to its thermodynamic equilibrium with the solvent water. In order to increase the refrigerant's purity, the vapor is partially condensed in a dephlegmator. In this process, water accumulates predominantly in the liquid phase. This fluid is separated in the separator after the dephlegmator (21) and is fed back to the generator (15). The refrigerant vapor is led to the condenser (1).

The locations of the measuring sensors are also shown in Figure 1. For temperature measurement, Pt100 sensors with an accuracy class of 1/10B are installed in the external circuits. Thus, a high accuracy for determining the heat flow of the absorption heat pump is achieved. For safety reasons, pipe-mounted Pt100 sensors of an accuracy class of 1/3B are used to measure the temperatures in the refrigerant and solution circuits. By using measured density, pressure and temperature, the ammonia mass fraction of the refrigerant and the solutions can be determined by the equation of state of (Tillner-Roth and Friend 1998). The density of the weak solution and the refrigerant is measured in parallel to the expansion valves with one Coriolis mass flow meter each. For the density measurement of the strong solution, a Coriolis mass flow meter is installed in parallel to the solution heat exchanger. The mass flow through the Coriolis is approx. 2 kg/h. Due to the low mass flow, the heat transfer in the solution heat exchanger is almost unaffected. The advantage of this setup is that the pressure loss of the Coriolis mass flow meter has no influence on the process. However, the mass flow of the solutions cannot be measured.

For the calculation of the total uncertainty, the uncertainties of each measurement system, given in Table 1, were used. The method given in Eq. (1) is used to calculate the uncertainty σ of the measured values, e.g. p, T and ρ , to the state variables, e.g. ξ . In this work, the partial derivatives used in Eq. (1) are calculated as central difference. An example for the central difference of the ammonia mass fraction ξ with respect to the temperature T is given in Eq. (2), assuming that the uncertainty σ_T is used as temperature difference $\Delta T = \sigma_T$.

$$\sigma_\xi = \pm \sqrt{\left(\frac{\partial \xi}{\partial T} \sigma_T\right)^2 + \left(\frac{\partial \xi}{\partial p} \sigma_p\right)^2 + \left(\frac{\partial \xi}{\partial \rho} \sigma_\rho\right)^2} \quad \text{Eq. (1)}$$

$$\frac{\partial \xi}{\partial T} = \frac{\xi(p, T + \Delta T, \rho) - \xi(p, T - \Delta T, \rho)}{2\Delta T} \quad \text{Eq. (2)}$$

In order to optimize an absorption heat pump, it is of interest to maximize the absorption and desorption efficiency. The absorption efficiency is defined in Eq. (3) as the ratio of the achieved change of the ammonia mass fraction in the absorber ($\xi_{ss}^{\rho, \vartheta, p} - \xi_{ws}^{\rho, \vartheta, p}$) with respect to the change of the ammonia mass fraction in an ideal absorber ($\xi_{ss}^{x=0, \vartheta, id, p} - \xi_{ws}^{\rho, \vartheta, p}$). Similarly, the desorption efficiency is defined in Eq. (4) as the ratio of the achieved change of the ammonia mass fraction in the generator ($\xi_{ss}^{\rho, \vartheta, p} - \xi_{ws}^{\rho, \vartheta, p}$) with respect to the change of the ammonia mass fraction in an ideal generator ($\xi_{ss}^{\rho, \vartheta, p} - \xi_{ws}^{x=0, \vartheta, id, p}$).

$$\eta_{\xi, \text{abs}} = \frac{\xi_{ss}^{\rho, \vartheta, p} - \xi_{ws}^{\rho, \vartheta, p}}{\xi_{ss}^{x=0, \vartheta, id, p} - \xi_{ws}^{\rho, \vartheta, p}} \quad \text{Eq. (3)}$$

$$\eta_{\xi, \text{gen}} = \frac{\xi_{ss}^{\rho, \vartheta, p} - \xi_{ws}^{\rho, \vartheta, p}}{\xi_{ss}^{\rho, \vartheta, p} - \xi_{ws}^{x=0, \vartheta, id, p}} \quad \text{Eq. (4)}$$

In Eq. (3) and Eq. (4), the ideal states $\xi_{ss}^{x=0,\vartheta_{id},p}$ and $\xi_{ws}^{x=0,\vartheta_{id},p}$ are obtained from the ammonia-water equation of state for saturated liquid ($x = 0$) at the outlet of each plate heat exchanger. The assumption for the solution temperature ϑ_{id} is that an ideal heat exchange takes place, where the temperature difference at the pinch point is zero. However, these efficiencies neither locate the potentials in absorption or desorption nor do they show whether the measured ammonia mass fractions of the solutions are close to thermodynamic equilibrium or not. For this reason, the ammonia mass fractions of each solution are considered directly and the efficiencies are listed for comparability with other works.

3. RESULTS AND CONCLUSIONS

The experimental tests were performed with four operating points of the absorption heat pump, which are shown in Table 2. The operating points have been selected within the project, described in detail in (Mirl et al. 2018a; Mirl et al. 2018b). However, findings on the absorber and on the generator can also be transferred to other operating points. The external inlet temperatures of the evaporator $\vartheta_{ext,evap,in}$ and the generator $\vartheta_{ext,gen,in}$ are set and controlled direct by the external temperature control units. The heat capacity rate of these circuits was set to $\dot{W}_{evap} = \dot{W}_{gen} = 0.8 \text{ kW/K}$ and kept constant. The external inlet temperature at the absorber $\vartheta_{ext,abs,in}$ is also controlled direct by the dry heat rejection unit. The external outlet temperature at the condenser $\vartheta_{ext,cond,out}$, however, is set by reducing the external mass flow rate $\dot{M}_{ext,cond}$. Due to a series connection, the mass flow rate in the absorber $\dot{M}_{ext,abs} = \dot{M}_{ext,cond}$ was also varied. As shown by Triché et al. (2017), a decreasing external mass flow rate reduces the absorption.

The measured values are recorded every 5 seconds over a period of 30 minutes under stable operating conditions. From this, time averages are formed. Those time-averaged values are used for further process evaluation. In order to find the optimal low-pressure level of the heat pump, the low-pressure was varied for each operating point and only those measurements with the highest coefficient of performance are used.

In order to identify the potentials of the absorber and the generator, the ammonia mass fractions of the strong and the weak solution are analyzed for each operating point. The results are presented in Figure 2. The operating points are shown on the x-axis and the ammonia mass fraction is shown on the y-axis. For each operating point, six ammonia mass fractions are calculated: three for the strong solution (ss) and three for the weak solution (ws). The ammonia mass fraction calculated from the measured density ρ of each solution is in the middle of each bar, i.e. $\xi_{ss}^{\rho,\vartheta,p}$, $\xi_{ws}^{\rho,\vartheta,p}$. The ammonia mass fractions $\xi_{ss}^{x=0,\vartheta,p}$ and $\xi_{ws}^{x=0,\vartheta,p}$ are calculated values by using the measured temperature ϑ and pressure p and assuming that the solution at the outlet of the heat exchanger is a saturated liquid at thermodynamic equilibrium $x = 0$. The highest value for the ammonia mass fraction $\xi_{ss}^{x=0,\vartheta_{id},p}$ is the ammonia mass fraction of the strong solution for ideal heat and mass transfer within the absorber. This value is calculated as saturated liquid with given pressure p_{low} and an outlet temperature of the strong solution $\vartheta_{ss,abs,out}$, which is equal to the inlet temperature of the external circuit $\vartheta_{ext,abs,in}$. Hence, this value corresponds to the ammonia mass fraction of the strong solution, which can be achieved in an ideal absorber. The lowest ammonia mass fraction $\xi_{ws}^{x=0,\vartheta_{id},p}$ of each bar is calculated as saturated liquid at high pressure for an ideal generator.

Regarding the optimization of the absorber and the generator, the differences between the ammonia mass fractions can be interpreted as potentials in absorption or desorption. The differences in the ammonia mass fractions obtained from measured densities $\xi^{\rho,\vartheta,p}$ and those obtained by using the

Table 2. Operating points of the absorption heat pump

Operating Point	$\vartheta_{ext,gen,in}$	$\vartheta_{ext,evap,in}$	$\vartheta_{ext,cond,out}$	$\vartheta_{ext,abs,in}$	$\dot{M}_{ext,abs}$
1	110 °C	42 °C	52 °C	40 °C	0.45 kg/s
2	110 °C	30 °C	43 °C	28 °C	0.41 kg/s
3	100 °C	42 °C	52 °C	40 °C	0.31 kg/s
4	100 °C	30 °C	43 °C	28 °C	0.33 kg/s

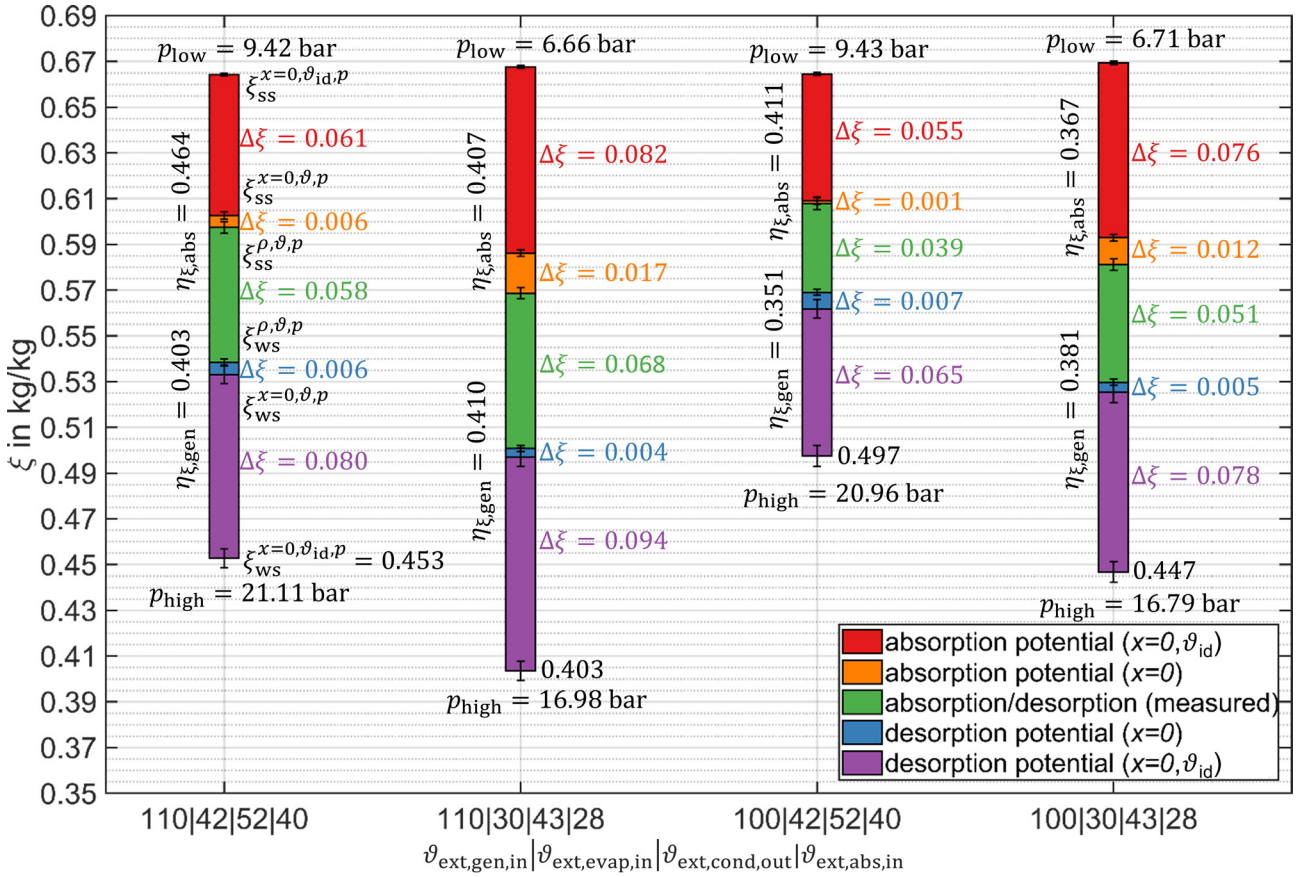


Figure 2: analysis of the ammonia mass fractions of the strong and weak solution

saturated liquid condition $\xi^{x=0, \vartheta, p}$ indicate the potentials in mass transfer within the generator unit and the absorber. For the generator unit, this potential is $0.004 < \Delta\xi < 0.007$ and is therefore within the measurement uncertainty at almost every operating point. In this regard, the generator unit works well. For the absorber, however, the difference of the ammonia mass fraction is in the range of $0.001 < \Delta\xi < 0.017$ and is only in the third operating point within the measurement uncertainty. Hence, there is a potential in mass transfer that could increase the current absorber efficiency for example at operating point 2 from $\eta_{\xi,abs} = 0.407$ by $\Delta\eta_{\xi,abs} = 0.102$.

For both, absorber and generator, the differences between $\xi^{x=0, \vartheta_{id}, p}$ and $\xi^{x=0, \vartheta, p}$ are larger in every operating point than the achieved absorption and desorption, respectively. Since $\xi^{x=0, \vartheta_{id}, p}$ is dominantly influenced by the temperature, the coupled heat and mass transfer within the heat exchangers has the highest optimization potential.

For this reason, the heat transfer within the heat exchangers is analyzed more detailed for operating point 2. Therefore, the heat exchangers are divided into $n = 200$ cells with the same heat transfer area A and overall heat transfer coefficient k . The heat transfer equation Eq. (5) is solved for each cell. With Eq. (6) and Eq. (7), the total transferred heat \dot{Q} as well as the mean temperature difference of heat transfer are calculated. With the measured temperatures and the measured total transferred heat \dot{Q} as boundary conditions, the system of equations can be solved iteratively. Hence, the temperature profiles within the heat exchangers can be calculated.

$$\dot{Q}_i = \frac{k \cdot A}{n} \cdot \theta_{m,i} = \dot{M} \cdot c_p \cdot \Delta\vartheta_i = \dot{M} \cdot \Delta h_i \quad \text{Eq. (5)}$$

$$\theta_m = \frac{1}{n} \sum_{i=1}^n \theta_{m,i} = \frac{1}{n} \sum_{i=1}^n \frac{(\vartheta_{1,in} - \vartheta_{2,out})_i + (\vartheta_{1,out} - \vartheta_{2,in})_i}{2} \quad \text{Eq. (6)}$$

$$\dot{Q} = \sum_{i=1}^n \dot{Q}_i = k \cdot A \cdot \theta_m \quad \text{Eq. (7)}$$

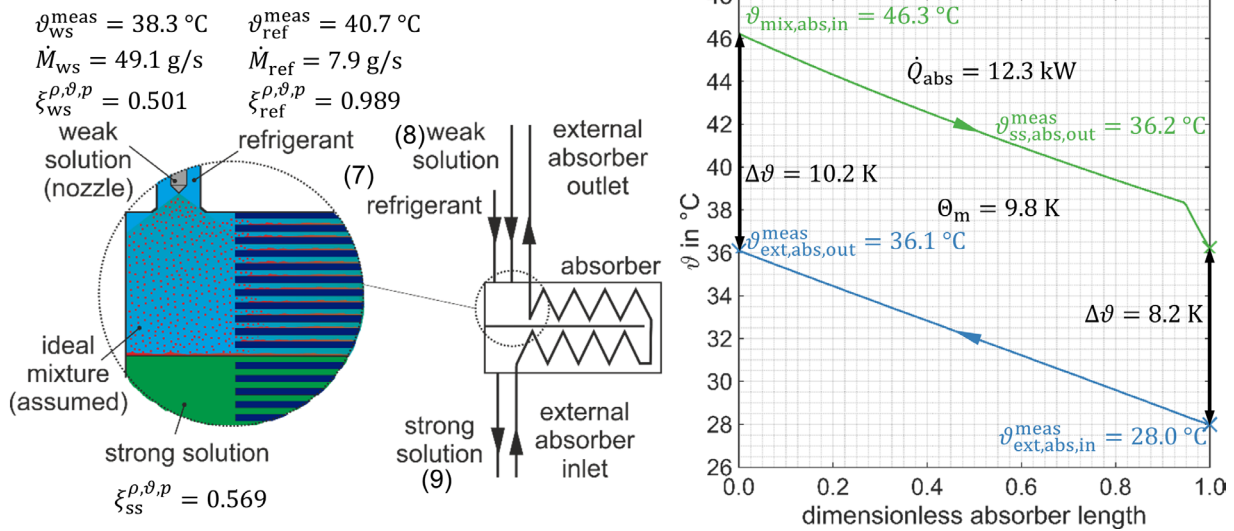


Figure 3: analysis of the temperature profile of the absorber at operating point 2 (110|30|43|28)

The resulting temperature profiles as well as the schematic design of the absorber are shown in Figure 3. For the calculation of the temperature profiles, the two fluids are assumed to be optimally mixed by spraying the weak solution into the refrigerant vapor at the inlet of the absorber. Hence, the inlet temperature of the mixture $\vartheta_{mix,abs,in}$ can be calculated by the energy balance and thermodynamic equilibrium of the two-phase mixture. The calculated temperature profiles within the absorber are shown in Figure 3 on the right. The dimensionless absorber length is plotted on the x-axis and the temperature is plotted on the y-axis. The measured fluid temperatures are highlighted by the superscript “meas”. The temperature of the ammonia water mixture decreases continuously during heat transfer due to the thermodynamic equilibrium within the two-phase region. The higher temperature decrease of the strong solution in the area of the dimensionless absorber length of > 0.95 is caused by the subcooling of the solution. However, by controlling the pump storage tank to a constant liquid level, vapor from the absorber must also enter the pump storage tank. This indicates that either the distribution of the strong solution on the plate channels is uneven or the liquid phase near the wall is actually subcooled. Hence, there is not enough surface available for mass transfer. Regarding heat transfer, the mean temperature difference of the heat transfer is high at $\theta_m = 9.8\text{ K}$. Therefore, the absorber has to be optimized regarding a higher total heat transfer and a better distribution of the flow to the plate channels. A higher heat transfer can be achieved by increasing the absorber length.

Analogous to Figure 3, the temperature profile of the generator at operating point 2 are presented in Figure 4. The strong solution enters the generator at saturated state. Analogous to the absorber, the temperature of the solution changes along the generator length, due to the thermodynamic

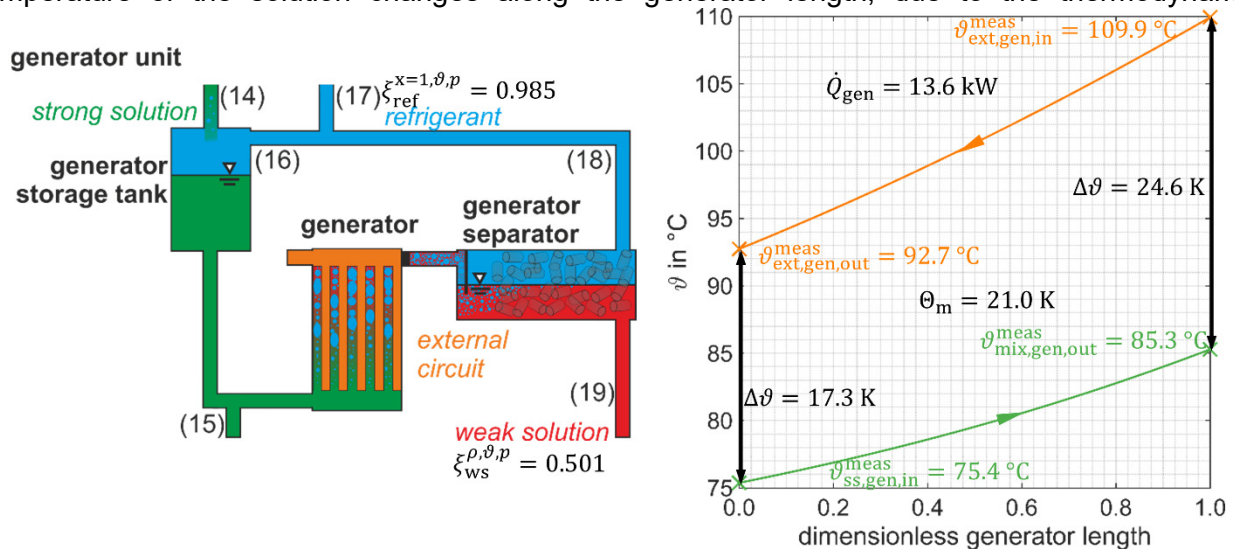


Figure 4: analysis of the temperature profile of the generator at operating point 2 (110|30|43|28)

equilibrium. However, the temperature difference in the external circuit is lower. Hence, the pinch point of the heat transfer is present at the inlet of the weak solution and is $\Delta\vartheta = 17.3$ K. This shows that the maximum potential of desorption will be even higher if the external mass flow is increased. However, one aim of Mirl et al. (2018b) is to maximize the temperature difference of the external fluid. Therefore, the mass flow has to be low. Hence, in order to decrease the high mean temperature difference in the generator of $\Theta_m = 21.0$ K and thereby to increase desorption process, the overall heat transfer coefficient or the heat transfer area have to be increased. Since the plate heat exchanger already consists of 60 plates, it is not appropriate to increase the heat transfer area by adding additional plates. Instead, a direct flow through the plate heat exchanger in conjunction with a multi-pass plate heat exchanger should be investigated to increase the overall heat transfer coefficient.

4. SUMMARY

Experimental investigations to identify and classify optimization potentials in heat and mass transfer of the absorber and generator were performed. For this purpose, the ammonia mass fractions of the strong and weak solution were analyzed at four operating points. This analysis revealed that the absorber efficiency is $0.367 \leq \eta_{\xi,abs} \leq 0.464$ and the generator efficiency is $0.351 \leq \eta_{\xi,gen} \leq 0.410$. Hence, the unused potentials in absorption and desorption process at the current state are higher than the achieved degassing range. It was also shown, that the potential in mass transfer at the outlet of the generator unit is $\Delta\xi \leq 0.007$ and therefore almost in thermodynamic equilibrium at all operating points. There is currently no need for enhancing the mass transfer at the generator unit. A more detailed evaluation of the data showed, that the highest potential for the optimization of the absorber and generator is within the combined heat and mass transfer at the inside of the plate heat exchangers. The potentials were determined by using calculated temperature profiles. The mean temperature of heat transfer at the absorber is $\Theta_m = 9.8$ K and for the generator $\Theta_m = 21.0$ K. From these analyses, it is pointed out, that the absorber has to be optimized with regard to a uniform distribution of the weak solution and refrigerant vapor to the plate channels as well as to a higher overall heat transfer. At the generator, the heat transfer must also be improved. The use of a direct flow multi-pass plate heat exchanger was suggested as an optimization proposal for the generator.

ACKNOWLEDGEMENTS

The work is based on a project (funding code "19696 N/2") which is supported within the scope of the "program for promoting joint industrial research (IGF)" by the German Federal Ministry of Economic Affairs and Energy (Bundesministerium für Wirtschaft und Energie, BMWi) on the basis of a decision by the German Bundestag via the Federation of Industrial Research Associations (Arbeitsgemeinschaft industrieller Forschungsvereinigungen, AiF). The authors would like to thank them sincerely for their support.

NOMENCLATURE

A	heat transfer area (m ²)	c_p	specific heat capacity (kJ/(kg·K))
h	specific enthalpy (kJ/kg)	k	overall heat transfer coefficient
\dot{M}	mass flow rate (kg/s)	n	number of cells
p	pressure (bar)	\dot{Q}	heat flow (kW)
T	temperature (K)	\dot{W}	heat capacity rate (kW/K)
w	velocity (mm/s)	x	vapor quality
Δ	difference	$\eta_{\xi,abs}$	absorption efficiency (-)
$\eta_{\xi,gen}$	desorption efficiency (-)	ϑ	temperature (°C)
Θ_m	mean temperature in heat transfer (K)	ρ	density (kg/m ³)
σ	uncertainty in measurement of the variable	ξ	ammonia mass fraction (-)

Subscripts

1	heat-emitting flow	2	heat-absorbing flow
abs	absorber	cond	condenser
evap	evaporator	ext	external circuit
gen	generator	high	high level
i	count index	id	ideal heat exchanger
in	inlet	low	low level
mix	mixture	out	outlet
ref	refrigerant	ss	strong solution
ws	weak solution		

Superscripts

<i>meas</i>	measured value	ρ, ϑ, p	calculated with use of ρ, ϑ, p
$x = 0, \vartheta, p$	calculated with use of $x = 0, \vartheta, p$	$x = 1, \vartheta, p$	calculated with use of $x = 1, \vartheta, p$
$x = 0, \vartheta_{id}, p$	calculated with use of $x = 0, \vartheta_{id}, p$		

REFERENCES

- Aprile, M., Scoccia, R., Toppi, T., Guerra, M., Motta, M. 2016 Modelling and experimental analysis of a GAX NH₃–H₂O gas-driven absorption heat pump. *Int. J. Refrig.* 66, pp. 145–155.
- Castro, J., Oliet, C., Rodríguez, I., Oliva, A. 2009 Comparison of the performance of falling film and bubble absorbers for air-cooled absorption systems. *Int. J. Therm. Sci.* 48 (7), pp. 1355–1366.
- Cerezo, J., Best, R., Bourouis, M., Coronas, A. 2010 Comparison of numerical and experimental performance criteria of an ammonia–water bubble absorber using plate heat exchangers. *Int. J. Heat Mass Transf.* 53 (17-18), pp. 3379–3386.
- Mirl, N., Schmid, F., Spindler, K. 2018a Experimentelle Untersuchung zur Einbindung einer Ammoniak-Wasser Absorptionswärmepumpe in Fernwärmenetze: Jahrestagung des Deutschen Kälte- und Klimatechnischen Vereins. Aachen, Germany, AA II.1.11.
- Mirl, N., Schmid, F., Spindler, K. 2018b Reduction of the return temperature in district heating systems with an ammonia-water absorption heat pump. *Case Studies in Thermal Engineering* (12), pp. 817–822.
- Mittermaier, M., Ziegler, F. 2015 Theoretical evaluation of absorption and desorption processes under typical conditions for chillers and heat transformers. *Int. J. Refrig.* 59, pp. 91–101.
- Müller, M., Spindler, K. 2013 Effizienzsteigerung einer Ammoniak/Wasser-Absorptionskältemaschine: Jahrestagung des Deutschen Kälte- und Klimatechnischen Vereins. Hannover, Germany, AA II.1.08.
- Paar, A., Herbert, F., Pehnt, M., Ochse, S., Richter, S., Maier, S. et al. 2013 Transformationsstrategien von fossiler zentraler Fernwärmeversorgung zu Netzen mit höheren Anteilen erneuerbarer Energien. Heidelberg, Germany.
- Said, S.A.M., Spindler, K., El-Shaarawi, M. A., Siddiqui, M. U., Schmid, F., Bierling, B., Khan, M.M.A. 2016 Design, construction and operation of a solar powered ammonia–water absorption refrigeration system in Saudi Arabia. *Int. J. Refrig.* 62, pp. 222–231.
- Staedter, M. A., Garimella, S. 2018 Thermodynamic considerations for optimal thermal compressor design. *Int J Ref* 91, pp. 28–38.
- Tillner-Roth, R., Friend, D. G. 1998 A Helmholtz Free Energy Formulation of the Thermodynamic Properties of the Mixture {Water + Ammonia}. *J. Phys. Chem. Ref. Data* 27 (1), pp. 63–96.
- Triché, D., Bonnot, S., Perier-Muzet, M., Boudéhen, F., Demasles, H., Caney, N. 2017 Experimental and numerical study of a falling film absorber in an ammonia-water absorption chiller. *Int. J. Heat Mass Transf.* 111, pp. 374–385.
- Venegas, M., Rodríguez, P., Lecuona, A., Izquierdo, M. 2005 Spray absorbers in absorption systems using lithium nitrate–ammonia solution. *Int. J. Refrig.* 28 (4), pp. 554–564.